Available online at www.sciencedirect.com

ScienceDirect

journal homepage: www.elsevier.com/locate/AJPS

Original Research Paper

Co-amorphous solid dispersion systems of lacidipine-spironolactone with improved dissolution rate and enhanced physical stability

*Zhaomeng Wang [a], Mengchi Sun [a], Tian Liu [a], Zisen Gao [b], Qing Ye [a], Xiao Tan [a], Yanxian Hou [a], Jin Sun [a], Dun Wang [b,**], Zhonggui He [a,*]*

[a] *Wuya College of Innovation, Shenyang Pharmaceutical University, Shenyang 110016, China*
[b] *Key Laboratory of Structure-Based Drug Design & Discovery of Ministry of Education, Shenyang Pharmaceutical University, Shenyang 110016, China*

ARTICLE INFO

ABSTRACT

Co-amorphous solid dispersion (C-ASD) systems have attracted great attention to improve the solubility of poorly soluble drugs, but the selection of an appropriate stabilizer to stabilize amorphous forms is still a huge challenge. Herein, C-ASD system of two clinical combined used drugs (lacidipine (LCDP) and spironolactone (SPL)) as stabilizers to each other, was prepared by solvent evaporation method. The effects of variation in molar ratio of LCDP and SPL (3:1, 1:1, 1:3, 1:6, and 1:9) on the drug release characteristics were explored. Polarized light microscopy (PLM), powder X-ray diffraction (PXRD), differential scanning calorimetry (DSC) and thermogravimetric analysis (TGA) were employed to evaluate the solid states. Prepared C-ASDs were further studied for their stability under the high humidity (RH 92.5%). Further analysis of C-ASDs via Fourier-transform infrared spectroscopy (FTIR) and Raman spectroscopy confirmed that hydrogen bond interactions between the two drugs played a significant role in maintaining the stability of the C-ASDs systems. Moreover, molecular dynamic (MD) simulations provided a clear insight into the stability mechanism at the molecular level. This study demonstrated the novel drug-drug C-ASDs systems is a promising formulation strategy for improved dissolution rate and enhanced physical stability of poorly soluble drugs.

---

* Corresponding author at: Wuya College of Innovation, Shenyang Pharmaceutical University, No. 103, Wenhua Road, Shenyang 110016, China. Tel.:+86 24 23986321.
** Corresponding author at: Key Laboratory of Structure-Based Drug Design & Discovery of Ministry of Education, Shenyang Pharmaceutical University, No. 103, Wenhua Road, Shenyang 110016, China. Tel.:+86 24 23986428.
E-mail addresses: wangduncn@hotmail.com (D. Wang), hezhgui_student@aliyun.com (Z. He).
Peer review under responsibility of Shenyang Pharmaceutical University.

1. Introduction

Many new drug candidates identified by current drug discovery techniques are poorly water soluble [1]. This drawback obviously impairs the oral bioavailability of these candidates [2]. Thus, several formulation strategies are adopted to settle the rough issue, such as cyclodextrin inclusion complexes [3], nanocrystals [4], nanoemulsions [5] and amorphous solid dispersions [6], etc.

Amorphous solid dispersions (ASDs) have been a preferable method to enhance the solubility and the dissolution rate [7]. However, an amorphous system is easily transformed into the crystalline form due to its higher free energy and poor thermodynamical stability, which would weaken the dominant solubility advantages conferred by amorphization [8]. To maintain the stability of this system, a suitable stabilizer is needed. Polymers are usually used as stabilizers for ASDs, but the following problems are found: (a) high hygroscopicity of polymers would increase the plasticization effect of the amorphous systems and decrease the physical stability; (b) low drug loading could increase the final dosage unit volume, limiting the clinic application; (c) large amounts of polymers might have excipient-associated side effects [9,10].

Co-amorphous solid dispersions (C-ASDs) systems containing small molecular weight stabilizers have been emerging as a more promising strategy to solve this issue in recent years [11]. Many small-molecule stabilizers such as saccharin, citric acid, tartaric acid, and amino acids, have been selected as co-formers to stabilize the amorphous systems [12–14]. In addition, many pharmacologically relevant drug-drug C-ASDs systems have also been reported. For example, simvastatin and glipizide, indomethacin and naproxen, atenolol and hydrochlorothiazide C-ASDs systems, showed a huge advantage in solubility, dissolution rate and physical stability [15–17].

In this study, two water-insoluble drugs possessing pharmacological synergy, lacidipine (LCDP, Fig. 1A) and spironolactone (SPL, Fig. 1B), were chosen to establish the C-ASDs system. LCDP is a dihydropyridine calcium antagonist as a first-line drug for the therapy of hypertension [18], and SPL is an aldosterone antagonist and has diuretic and antihypertensive effect [19]. This combined use of both antihypertensive agents with different mechanisms have proved fewer adverse effects for individualized treatment in clinic [20]. Herein, the *in vitro* release assays and a series of solid characterization methods were employed to confirm the formation of the C-ASDs systems and to select the optimal molar ratio of LCDP and SPL for maintaining good physical stability under high humidity. Moreover, molecular dynamic (MD) simulations were employed as a complementary tool to provide insight into the specific stabilization mechanism at a molecular level for the drug-drug C-ASDs system.

2. Materials and methods

2.1. Materials

Lacidipine was purchased from Kangya of NingXia Pharmaceuticals Co. Ltd. (Ningxia, China). Spironolactone was purchased from Zhejiang Langhua Pharmaceutical Co. Ltd (Zhejiang, China). Tween 80 was obtained from Tianjin Bodi Chemical Holding Co. Ltd (Tianjin, China). Methanol (HPLC grade) was purchased from Kangkede Tianjin Co. Ltd (Tianjin, China). Deionized distilled water was used throughout the study.

2.2. Preparation of co-amorphous solid dispersion systems

C-ASDs samples were prepared by solvent evaporation. LCDP and SPL in different molar ratios (3:1, 1:1, 1:3, 1:6, and 1:9) were dissolved in ethanol and rotavaporized at 30 °C, and the samples were dried under vacuum for 24 h to remove residual solvent. The resulting amorphous material was ground with a mortar and pestle and then forcibly passed through 80 mesh sieves to yield a uniform, free flowing powder. In addition, pure amorphous LCDP and pure amorphous SPL were prepared in the same procedure. The amorphous physical mixture was prepared by the method of increment by equal quantity.
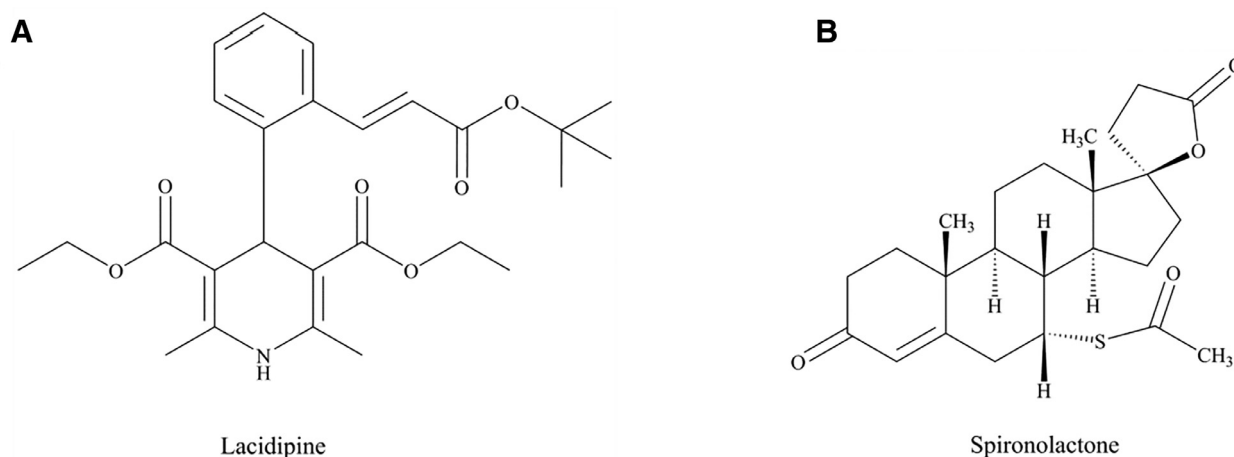

Fig. 1 – Chemical structures of (A) lacidipine (LCDP) and (B) spironolactone (SPL).

2.3. Physical stability study

The C-ASDs systems in different molar ratios (3:1, 1:1, 1:3, 1:6, and 1:9) were exposed to saturated potassium nitrate solutions (RH 92.5%) in a dessicator. After 10 d, the samples were withdrawn, and the stability of the C-ASDs systems was further analyzed by PXRD, PLM, FTIR, and *in vitro* release test.

2.4. Solid state characterization

2.4.1. Polarized light microscopy (PLM)
Images of C-ASDs samples in different molar ratios (3:1, 1:1, 1:3, 1:6, and 1:9) were collected using PLM (Olympus Corporation., Tokyo, Japan) at different time points: (i) immediately after obtaining the dried material; (ii) 10 d post exposed to high humidity (RH 92.5%). Samples were sprinkled onto a glass slide and then covered with a glass coverslip. Images of C-ASDs samples were collected using $4 \times$ magnification.

2.4.2. Powder X-ray diffraction (PXRD)
Powder X-ray diffraction (Rigaku Corporation, Tokyo, Japan) was used to evaluate the solid-state characteristics of C-ASDs systems. Cu Kα radiation (1.54 Å; 40 kV $\times$ 30 mA) was used, and data were collected in the range of 3–50° 2θ with a dwell time of 0.2 s and a step size of 0.02°

2.4.3. Differential scanning calorimetry (DSC)
A DSC 1 (Mettler-Toledo International Inc., Switzerland) was used to analyze the thermal behavior of crystalline drugs and C-ASDs samples. Approximately 4 mg sample was sealed in aluminum pans with perforated lids, under the nitrogen gas at a flow rate of 40 ml/min, the samples were heated at a rate of 10 °C /min from 25 °C to 230 °C to obtain DSC thermograms.

2.4.4. Thermogravimetric analysis (TGA)
The TGA analysis was performed by using TGA 550 (TA instrument-Waters LLC). Under nitrogen purge with a flow rate of 25 ml/min, samples were heated from room temperature to the desired temperature at a heating rate of 10 °C /min.

2.4.5. Fourier-transform infrared spectroscopy (FTIR)
To investigate the molecular interactions between LCDP and SPL, Fourier-transform infrared spectroscopy (Bruker Corporation, Switzerland) was used to obtain the spectra of crystalline LCDP, crystalline SPL and C-ASDs systems in different molar ratios (3:1, 1:1, 1:3, 1:6, and 1:9) from the spectral region 4000–400 cm^{-1} with a resolution of 4 cm^{-1}. Samples were prepared by grounding with KBr gently and respectively.

2.4.6. Raman spectroscopy
The existence form of LCDP and SPL in different LCDP-SPL C-ASDs system was assessed by Raman spectroscopy. C-ASDs samples in different molar ratios (3:1, 1:1, 1:3, 1:6, and 1:9) were analyzed *in situ* through a quartz sight window via a Raman spectrometer (in Via Laser Micro Raman Spectroscopy, Renishaw PLC) equipped with a thermoelectrically cooled CCD detector and a fiber optic probe. The measurements were performed at room temperature with a laser wavelength of 785 nm and laser power of 500 mW.

2.5. In vitro release

A USP type II apparatus (ZRS-8G; Tianda Tianfa Technology Co., Ltd, Tianjin, China) was used to study the release of crystalline LCDP, crystalline SPL, amorphous physical mixture and C-ASDs systems in different molar ratios (3:1, 1:1, 1:3, 1:6, and 1:9) under physiological correlation medium (0.07% Tween 80) [21,22]. The powder sample 4 mg (LCDP equivalent) was dispersed by filling the powder in a capsule and suspending the capsule in the basket in 500 ml of release medium with a paddle speed of 50 rpm. 5 ml samples were withdrawn at 5, 10, 20, 30, 45, 60, and 120 min and replaced with the same amount of fresh medium to keep the volume constant. The samples were filtered with 0.22 μm microporous membrane, and 1 ml of the filtrate was diluted with the same volume of methanol, vortex blending and analyzed by HPLC. All experiments were performed in triplicate.

2.6. Molecular dynamics (MD) simulations

The structure of LCDP and SPL was created using Marvin sketch software. The 3D structures of both drugs were built by the structural minimization and the structural dynamics optimization via the Sybyl 6.9.1 software package (Tripos Associates: St.Louis, MO, 2003). The parameters of optimizing were following our previous work [23]. All other parameters were maintained at the default values. LCDP-SPL complexes were predicted by molecular docking using AutoDock 4.0 software. AutoDocking parameters were as follows: the maximum number of energy evaluations was 25 000 000 per run; the iterations of Solis and Wets local search were 3000; the number of generations was 100, and the number of individuals in population was 300 [24].

The LCDP-SPL complexes (1:1, 1:3, 1:6, and 1:9) were further optimized with the Material Studio 8.0 software. All molecular dynamics (MD) simulations were performed by using the Amorphous Cell and Forcite module of the Material Studio simulation package with COMPASS. In the MD simulations, the amorphous cell module was used to construct a box, which was inundated with 200 water molecules and different ratios of complexes. 100 ns MD simulations were performed under the constant temperature of 200 K.

2.7. HPLC conditions

The chromatographic separation was performed on a reverse phase Thermo Hypersil C$_{18}$ column (250 mm $\times$ 4.6 mm, 5 μm, Thermo Fisher Scientific Inc.) maintained at 30 °C. The mobile phase was composed of methanol and water (80:20, v/v). The flow rate was 0.8 ml/min and the detect wavelengths of LCDP and SPL were set at 284 nm and 238 nm, respectively.

2.8. Statistical analysis

SPSS statistics version 22 software was used to perform Unpaired *t*-test to determine any significant difference between the crystalline drug, physical mixture and LCDP-SPL C-ASDs systems in different molar ratios (3:1, 1:1, 1:3, 1:6, and 1:9). Differences were considered statistically significant when the P value was less than 0.05 ($P < 0.05$).
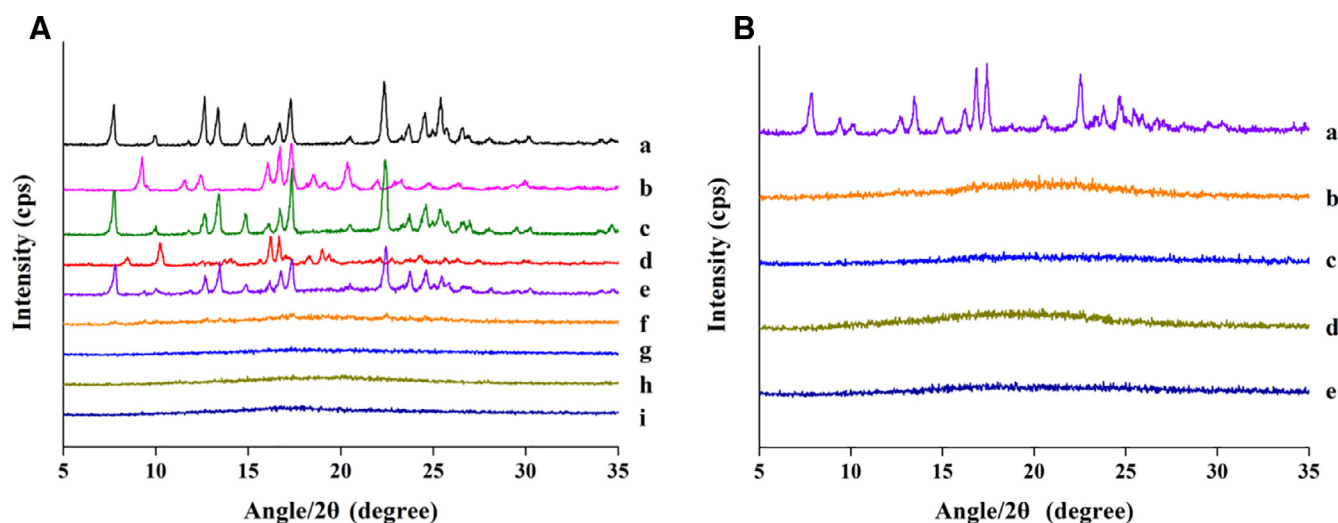
Fig. 2 – PXRD diffractograms of (A) (a) crystalline LCDP, (b) crystalline SPL, (c) crystalline LCDP subjected to solvent evaporation, (d) crystalline SPL subjected to solvent evaporation, and their C-ASDs system in different molar ratios freshly prepared (e) LCDP:SPL 3:1, (f) LCDP:SPL 1:1, (g) LCDP:SPL 1:3, (h) LCDP:SPL 1:6, and (i) LCDP:SPL 1:9. (B) C-ASDs system in different molar ratios exposed to high humidity (RH 92.5%) for 10 days. (a) LCDP: SPL 3:1, (b) LCDP: SPL 1:1, (c) LCDP: SPL 1:3, (d) LCDP: SPL 1:6, and (e) LCDP: SPL 1:9.

3.   Results and discussion

3.1.   Physical characterization of the LCDP- SPL C-ASDs systems

3.1.1.   Powder X-ray diffraction (PXRD)
PXRD was commonly used to determine the solid state of drugs. The crystallinity of crystalline LCDP, crystalline SPL, crystalline LCDP subjected to solvent evaporation, crystalline SPL subjected to solvent evaporation and all the freshly prepared LCDP-SPL C-ASDs were investigated by PXRD. As seen in Fig. 2A, the sharp peaks of the diffractograms for crystalline LCDP and crystalline SPL were detected. The single drug amorphous component could not be prepared via solvent evaporation, due to fast recrystallization during the process of preparation. The LCDP-SPL (3:1, 1:1) C-ASDs also showed the crystallinity peaks, but the degree of crystallinity was reduced. An amorphous halo was observed in the diffractogram for the investigated LCDP-SPL (1:3, 1:6, and 1:9) C-ASDs systems, suggesting that the crystalline drugs were converted into an amorphous form in these systems.

The C-ASDs were firstly exposed to high humidity and then subjected to PXRD as well. In the PXRD diffractograms, no detectable crystalline peak was observed for the LCDP-SPL (1:3, 1:6, and 1:9) C-ASDs systems, indicating that these C-ASDs systems were stable after exposure to high humidity, as shown in Fig. 2B.

3.1.2.   Thermal analysis
DSC was conducted to further confirm the crystalline nature of samples. Thermograms of the crystalline LCDP and crystalline SPL after the first and second heating are shown in Fig. S1, which revealed the Tg values of 59 °C and 92.16 °C for LCDP and SPL, respectively. As seen in Fig. S2, crystalline LCDP and crystalline SPL displayed sharp endothermic melting peaks at around 185.56 °C and 207.32 °C, respectively. The thermograms of physical mixture (1:6) and LCDP-SPL (3:1, 1:1) systems indicated that these compounds formed a binary eutectic system. In the total thermograms of LCDP-SPL (1:3, 1:6 and 1:9) systems, the melting peaks for LCDP and SPL were not observed, and they exhibited a single composition-dependent Tg value at 74.17 °C, 85.37 °C, and 92.87 °C, respectively. More importantly, it was noteworthy that with higher molar ratio of SPL, the C-ASDs systems showed Tg values close to Tg value of SPL, which was consistent with the statement that the Tg of the binary amorphous system tends to be close to the Tg of the component present in excess the mixture [25]. In addition, an exothermic event happened in the range of 120–150 °C, followed by endothermic peak at around 160–185 °C, which might be attributed to the recrystallization of amorphous drug and the melting of recrystallized drug, respectively.

TGA experiments were carried out to verify the impact of moisture or residual solvent on the C-ASDs systems. The TGA results demonstrated that LCDP and SPL are thermally stable within 189.1 °C and 219.64 °C, respectively. A small weight loss (0.77%) at about 78 °C was observed in the C-ASDs system (1:6), due to the residual ethanol in the C-ASDs system prepared by solvent evaporation (Fig. S3), which might lead to the lowered-Tg of C-ASDs system.

3.1.3.   Polarized light microscopy (PLM)
Polarized light microscopy (PLM) experiment was intuitively performed to evaluate the effect of humidity on the LCDP-SPL C-ASDs systems. In Fig. S4, birefringence phenomenon was obviously observed in crystalline LCDP and crystalline SPL, whereas no visible birefringence phenomenon was observed in all prepared LCDP-SPL C-ASDs systems except for the system with molar ratio of 3:1 and 1:1 in Fig. 3A. The re-
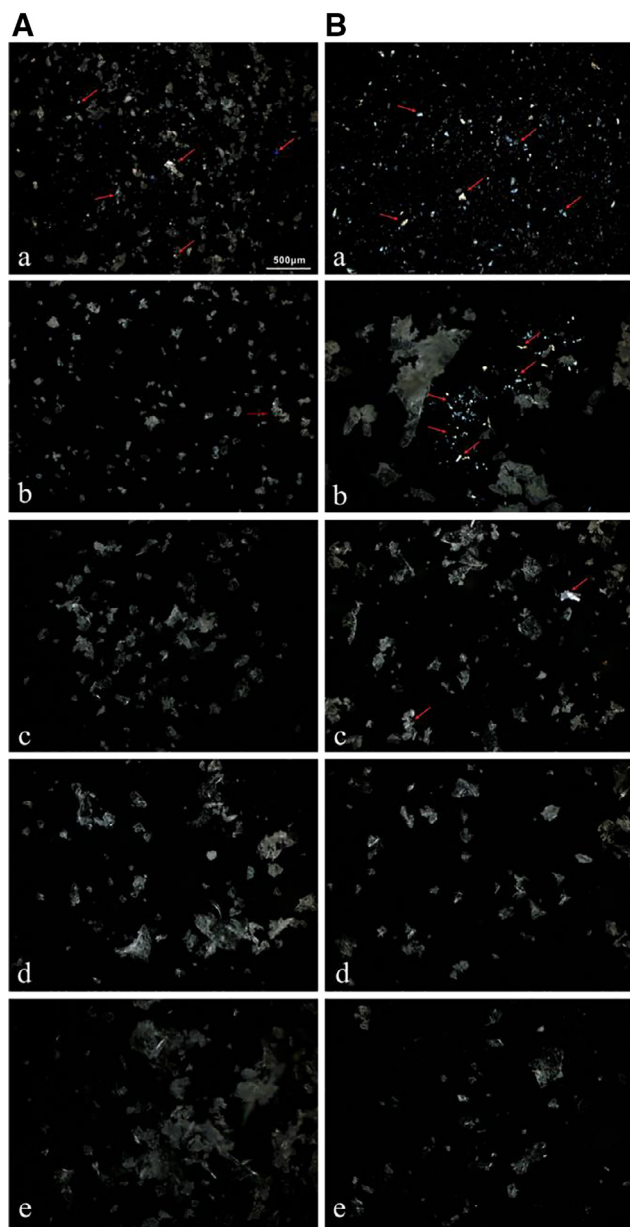
Fig. 3 – PLM images of LCDP-SPL C-ASDs systems (A) samples freshly prepared and (B) samples exposed to high humidity (RH 92.5%) for 10 days. (a) LCDP: SPL 3:1, (b) LCDP: SPL 1:1, (c) LCDP: SPL 1:3, (d) LCDP: SPL 1:6, and (e) LCDP: SPL 1:9.

sult was in a good agreement with the results obtained by PXRD. For the samples after exposure to high humidity in Fig. 3B, LCDP-SPL (1:6, 1:9) C-ASDs systems didn't exhibited birefringence signal, indicating that the excellent stability of both systems under this high humidity conditions. However, a few crystals were observed in the LCDP-SPL (1:3) C-ASDs systems. This phenomenon could not be detected by PXRD, due to the limited sensitivity. It was essential that a combination of several solid characterization methods was adopted to accurately determine the crystallinity states.

3.1.4. FTIR spectroscopy

FTIR was conducted to investigate the molecular interactions in the LCDP-SPL C-ASDs systems. The FTIR spectra of crystalline drugs and C-ASDs are presented in Fig. 4A. The crystalline LCDP showed the characteristic peak at 3348.3 cm^{-1}, belonging to the stretching vibration of the amino (–NH) groups [23]. And the crystalline SPL demonstrated strong bands of carbonyl (C=O) groups at 1691.1 cm^{-1}, 1768.1 cm^{-1} and 1674.1 cm^{-1}, assigned to the stretches of O=C–S, O=C–O and O=C–C=C, respectively. For the prepared C-ASDs systems, the peak intensity of amine groups was weakened in LCDP-SPL (3:1, 1:1) C-ASDs, while the distinctive amine peak of LCDP disappeared in the LCDP-SPL (1:3, 1:6 and 1:9) C-ASDs. Correspondingly, the carbonyl peak of the thioacetyl group in SPL was broadened and intensified in LCDP-SPL (1:1, 1:3, 1:6, and 1:9) C-ASDs systems, indicating the formation of intermolecular hydrogen bonds between the –NH group of the LCDP and the C=O group of thioacetyl in SPL. No intermolecular hydrogen bond in the LCDP-SPL (3:1) systems was formed.

The C-ASDs systems after exposure to high humidity could be further investigated using FTIR spectroscopy. As shown in Fig. 4B, the intensity of –NH peak at 3348.1 cm^{-1} in the LCDP-SPL (1:1) C-ASDs was enhanced. In the LCDP-SPL (1:3) C-ASDs system, a new peak at 3348.7 cm^{-1} was detected, corresponding to the –NH stretching peak of crystalline LCDP. In addition, the carbonyl peak of the thioacetyl group of SPL shifted from 1691.1 cm^{-1} to 1692.1 cm^{-1}. These changes indicated that these samples were recrystallized, and the intermolecular hydrogen bonds might be broken. In contrast, LCDP-SPL (1:6, 1:9) C-ASDs systems showed no notable differences in the spectra following storage at 92.5% RH for 10 d. The intermolecular hydrogen bonds in the LCDP-SPL (1:6, 1:9) C-ASDs were well maintained.

3.1.5. Raman spectroscopy

Raman spectroscopy is proved to be another efficient tool to analyze solid-state changes of drugs in the formulations and characterize the molecular interactions between drugs and excipients [26]. For the crystalline drug, the molecule structure is in a long-range order and the Raman-active bonds are indeed same in each molecule; however, the molecule structure of the amorphous state is in short-range order or lack in long-range order and represents relatively multiple regions [27]. Concerning to the prepared LCDP-SPL (1:1, 1:3, 1:6, 1:9) systems, C=O peak of the thioacetyl bond in SPL at 1691 cm^{-1} was broadened and shifted towards lower wavenumbers, and –NH stretching of crystalline LCDP at 3348.3 cm^{-1} disappeared in Fig. S5. These results suggested that the changes in molecular confirmation and confirmed the formation of intermolecular hydrogen bond interactions. Specifically, the –NH group of the LCDP and the O=C group of thioacetyl in SPL served as hydrogen bond donor and accepter, leading to the formation of a heterodimer. This result was consistent with the analysis of FTIR.

3.2. In vitro release

As shown in Fig. 5A, the release of low-amount drugs was detected from crystalline LCDP and its physical mixture. However, the release of LCDP from C-ASDs systems with all the
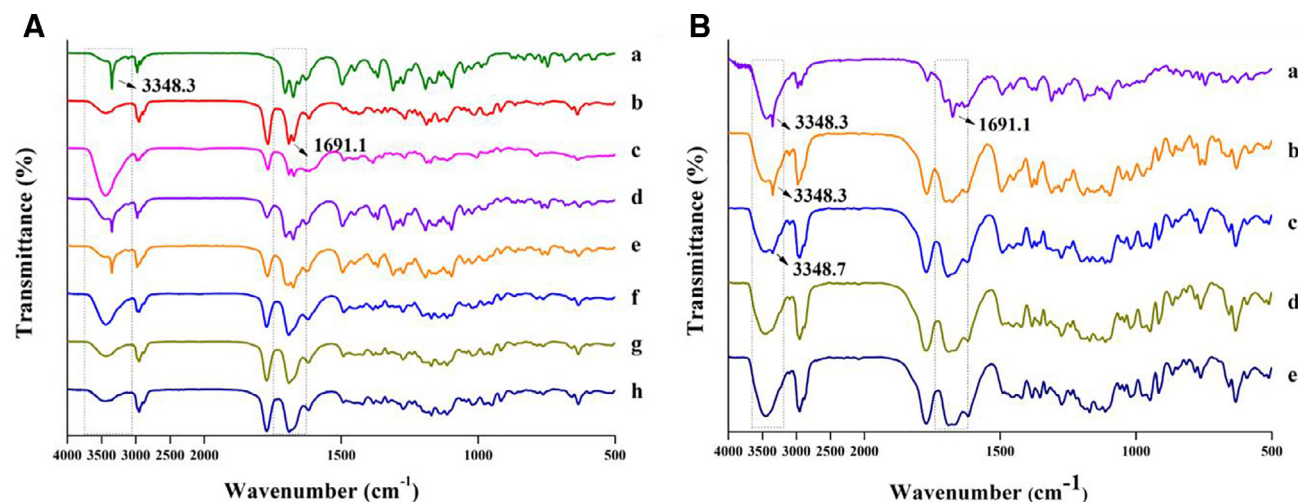
Fig. 4 – FTIR spectra of (A) (a) crystalline LCDP, (b) crystalline SPL, (c) physical mixture (1:6), and their C-ASDs systems in different molar ratios freshly prepared (d) LCDP: SPL 3:1, (e) LCDP: SPL 1:1, (f) LCDP: SPL 1:3, (g) LCDP: SPL 1:6, and (h) LCDP: SPL 1:9. (B) C-ASDs system in different molar ratios exposed to high humidity (RH 92.5%) for 10 d. (a) LCDP: SPL 3:1, (b) LCDP: SPL 1:1, (c) LCDP: SPL 1:3, (d) LCDP: SPL 1:6, and (e) LCDP: SPL 1:9.
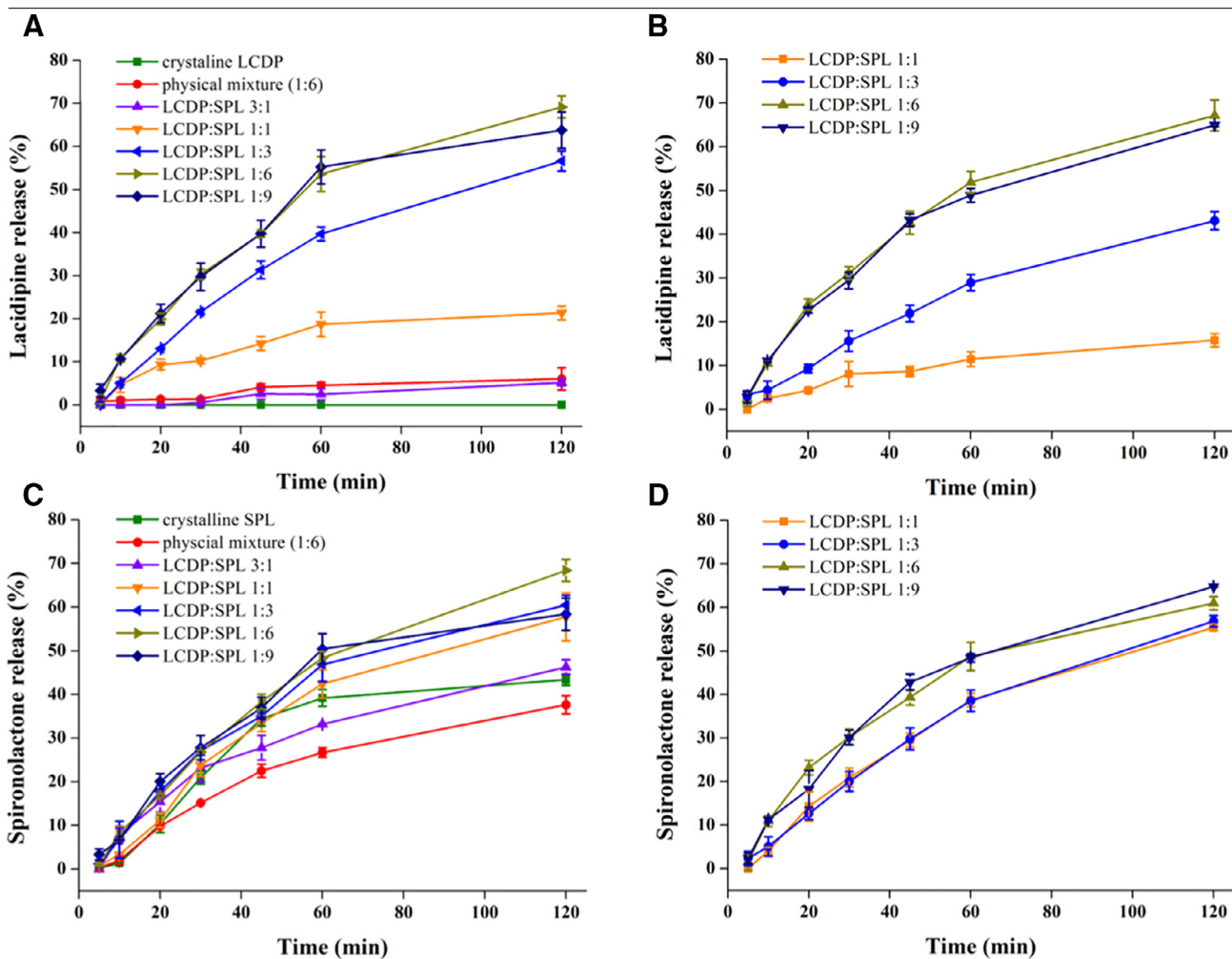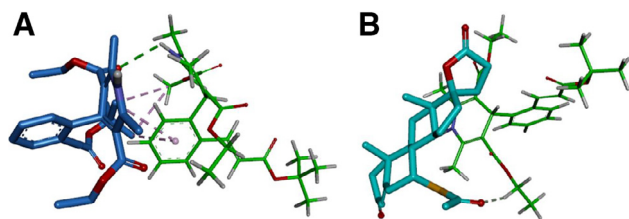

Fig. 5 – Release profiles of the: (A, C) LCDP and SPL from crystalline drug, physical mixture (1:6), and their C-ASDs system in different molar ratios. (B, D) LCDP and SPL from its C-ASDs systems under high humidity (RH 92.5%) for 10 days. Data are presented as the mean ± SD (n = 3).

Fig. 6 – Chemical structures with proposed hydrogen bond between (A) LCDP and LCDP, (B) LCDP and SPL.

different molar ratios was enhanced compared with its crude crystalline powders. The release rate and cumulative release of LCDP from different drug ratios C-ASDs have the considerable differences within 120 min. For LCDP-SPL C-ASDs with molar ratios (3:1, 1:1 and 1:3), the release of LCDP was 5.1%, 21% and 56%, respectively. This demonstrated that LCDP release would be enhanced when the content of SPL increased in the C-ASDs system. It was noteworthy that 69% of LCDP was released from LCDP-SPL (1:6) C-ASDs system within 120 min, similar to that of LCDP-SPL (1:9) C-ASDs system. Statistical data analysis revealed that there was no significant difference between these two systems ($P > 0.05$). Although both systems showed the maximum cumulative releases, LCDP-SPL (1:6) C-ASDs system was in closer proximity to the clinically relevant combination doses of 1:6.83 (4 mg/25 mg). Therefore, 1:6 was considered as the most optimal molar ratio to achieve the optimal release of LCDP-SPL C-ASDs system.

The releases of SPL from crystalline SPL, physical mixture, and LCDP-SPL system with the molar ratio of 3:1 were approximately 40% ($P > 0.05$) in Fig. 5C. The releases of SPL from LCDP-SPL (1:1, 1:3, 1:6, and 1:9) C-ASDs systems were found to be similar. The cumulative release of SPL from LCDP-SPL (1:6) C-ASDs system was nearly 1.5 times higher than that of the crystalline SPL.

To evaluate the physical stability of LCDP-SPL C-ASDs systems, the C-ASDs were subjected to the *in vitro* release test after exposure to high humidity (RH 92.5%). As seen in Fig.

5B and D, the significant decrease in the release of LCDP and SPL were observed in LCDP-SPL (1:1, 1:3) C-ASDs systems. This might be due to the recrystallization of amorphous drugs in C-ASDs. However, LCDP and SPL release profiles from both LCDP-SPL (1:6, 1:9) C-ASDs systems were similar to that of the freshly prepared samples ($P > 0.05$), indicating that LCDP-SPL (1:6, 1:9) C-ASDs systems showed exceptional stability under this high humidity conditions after 10 d. The amount of SPL was considered as a crucial factor influencing the stability. Hence, it is certainly believed that a suitable amount of stabilizer is necessary for a C-ASDs system to achieve the maximum release and good physical stability.

3.3. Molecular dynamic (MD) simulations

Molecular docking was performed to provide a better understanding of the molecular interactions. The hydrogen bonds between LCDP and LCDP (Fig. 6A), as well as between LCDP and SPL (Fig. 6B) were obviously observed. Docking results revealed that intermolecular hydrogen bonds were formed between the amine (–NH) group of LCDP and the carbonyl (C=O) of thioacetyl group in SPL, agreeing well with the experimental results of IR and Raman spectroscopy. Bulk amorphous cell models of LCDP and SPL were constructed (Fig. S6). In the computer simulations, the bond length and the binding energy were used to evaluate the strength of interactions. The bond length of –N–H•••O=C–O between two LCDP molecules was 2.82279 pm, whereas the bond length of –N–H•••O=S–O between LCDP and SPL was 2.83718 pm. Moreover, the binding energy value of hydrogen bond interaction in the LCDP-LCDP and LCDP-SPL complex was −2.8 kcal/mol and −4.2 kcal/mol, respectively. These results proved that LCDP had a higher tendency to interact with SPL through the formation of hydrogen bonds rather than aggregated between the individual molecules, which ultimately hindered the occurrence of recrystallization. Consequently, the –N–H•••O=S–O hydrogen bonds between LCDP and SPL molecule were the dominant force for stabilizing the LCDP-SPL C-ASDs systems.
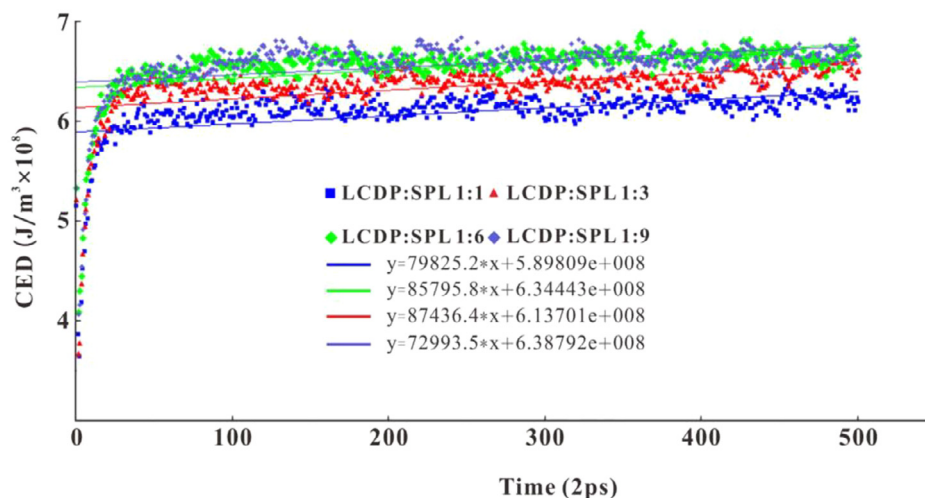
Fig. 7 – Cohesive energy density of LCDP-SPL C-ASDs systems as a function of simulation time.

In the MD simulation, cohesive energy density (CED) values were conducted to estimate the stability of systems, where higher values indicate better stability. Herein, the stability of different LCDP-SPL C-ASDs systems after exposure to high humidity was evaluated by CED values. As shown in Fig. 7, for LCDP-SPL (1:1, 1:3, 1:6 and 1:9) C-ASDs, the CED maximum value was 5.89809×10^8 J/m^3, 6.13701×10^8 J/m^3, 6.34443×10^8 J/m^3, and 6.38792×10^8 J/m^3, respectively. It could be seen that CED values increased along with the increased content of SPL in the C-ASDs system, while the CED reached the maximum value in LCDP-SPL (1:6, 1:9) C-ASDs systems. This trend was consistent with that of in vitro release results. Likewise, this was also confirmed by FTIR result that hydrogen bonds in the LCDP-SPL (1:1, 1:3) C-ASDs systems were impaired but were well maintained in LCDP-SPL (1:6, 1:9) C-ASDs systems.

Taken all together, both the results obtained experimentally and calculated theoretically elucidated that intermolecular hydrogen bond plays a significant role in maintaining the stability of LCDP-SPL C-ASDs system. Furthermore, MD simulations provided forceful evidence to help understand the stability mechanism at the molecular level.

4. Conclusion

LCDP-SPL C-ASDs systems were successfully established by solvent evaporation. The LCDP-SPL (1:6, 1:9) C-ASDs systems exhibited better in vitro release behaviors and physical stability than LCDP-SPL (1:1, 1:3) C-ASDs systems. Especially, the C-ASDs system with the optimal molar ratio of 1:6 was close to therapeutically relevant dose. FTIR and Raman spectroscopy revealed the formation of hydrogen bond between the –NH of LCDP and the O=C–S of SPL. The MD simulations further verified the formation of H-bonds and provided the calculated CED values for the C-ASDs systems in the presence of water molecules, which afforded a molecular level insight into the stability mechanism of the C-ASDs systems.

Declaration of interest

The authors report no conflicts of interest. The authors alone are responsible for the content and writing of this article.

Acknowledgments

Supplementary materials

Supplementary material associated with this article can be found, in the online version, at doi:10.1016/j.ajps.2018.11.001.

REFERENCES

[1] Chen H, Pui Y, Liu C, et al. Moisture-induced amorphous phase separation of amorphous solid dispersions: molecular mechanism, microstructure and its impact on dissolution performance. J Pharm Sci 2018;107(1):317–26.

[2] Horter D, Dressman JB. Influence of physicochemical properties on dissolution of drugs in the gastrointestinal tract. Adv Drug Deliv Rev 2001;46(1–3):75–87.

[3] Rudrangi SRS, Kaialy W, Ghori MU, Trivedi V, Snowden MJ, Alexander BD. Solid-state flurbiprofen and methyl-β-cyclodextrin inclusion complexes prepared using a single-step, organic solvent-free supercritical fluid process. Eur J Pharm Biopharm 2016;104:164–70.

[4] Guo M, Fu Q, Wu C, et al. Rod shaped nanocrystals exhibit superior in vitro dissolution and in vivo bioavailability over spherical like nanocrystals: a case study of lovastatin. Colloids Surf B Biointerfaces 2015;128:410–18.

[5] Pangeni R, Choi JU, Panthi VK, Byun Y, Park JW. Enhanced oral absorption of pemetrexed by ion-pairing complex formation with deoxycholic acid derivative and multiple nanoemulsion formulations: Preparation, characterization, and in vivo oral bioavailability and anticancer effect. Int J Nanomed 2018;13:3329–51.

[6] Li J, Wang X, Li C, et al. Viewing molecular and interface interactions of curcumin amorphous solid dispersions for comprehending dissolution mechanisms. Mol Pharm 2017;14(8):2781–92.

[7] Laitinen R, Lobmann K, Grohganz H, Priemel P, Strachan CJ, Rades T. Supersaturating drug delivery systems: the potential of co-amorphous drug formulations. Int J Pharm 2017;532(1):1–12.

[8] Edueng K, Mahlin D, Larsson P, Bergstrom CAS. Mechanism-based selection of stabilization strategy for amorphous formulations: insights into crystallization pathways. J Control Release 2017;256:193–202.

[9] Jensen KT, Larsen FH, Cornett C, Löbmann K, Grohganz H, Rades T. Formation mechanism of coamorphous drug–amino acid mixtures. Mol Pharm 2015;12(7):2484–92.

[10] Elder DP, Kuentz M, Holm R. Pharmaceutical excipients - quality, regulatory and biopharmaceutical considerations. Eur J Pharm Sci 2016;87:88–99.

[11] Dengale SJ, Grohganz H, Rades T, Löbmann K. Recent advances in co-amorphous drug formulations. Adv Drug Deliv Rev 2016;100:116–25.

[12] Newman A, Reutzel-Edens SM, Zografi G. Coamorphous active pharmaceutical ingredient-small molecule mixtures: considerations in the choice of coformers for enhancing dissolution and oral bioavailability. J Pharm Sci 2018;107(1):5–17.

[13] Fung M, Be Rzins KR, Suryanarayanan R. Physical stability and dissolution behavior of ketoconazole-organic acid coamorphous systems. Mol Pharm 2018;15(5):1862–9.

[14] Jensen KT, Larsen FH, Lobmann K, Rades T, Grohganz H. Influence of variation in molar ratio on co-amorphous drug-amino acid systems. Eur J Pharm Biopharm 2016;107:32–9.

[15] Lobmann K, Strachan C, Grohganz H, Rades T, Korhonen O, Laitinen R. Co-amorphous simvastatin and glipizide combinations show improved physical stability without evidence of intermolecular interactions. Eur J Pharm Biopharm 2012;81(1):159–69.

[16] Lobmann K, Laitinen R, Grohganz H, Gordon KC, Strachan C, Rades T. Coamorphous drug systems: enhanced physical stability and dissolution rate of indomethacin and naproxen. Mol Pharm 2011;8(5):1919–28.

[17] Moinuddin SM, Ruan S, Huang Y, et al. Facile formation of co-amorphous atenolol and hydrochlorothiazide mixtures via cryogenic-milling: enhanced physical stability, dissolution and pharmacokinetic profile. Int J Pharm 2017;532(1):393–400.

[18] Leonetti G. Clinical position of lacidipine, a new dihydropyridine calcium antagonist, in the treatment of hypertension. J Cardiovasc Pharmacol 1991;18(Suppl 11):S18–21.

[19] Mironneau J. Calcium channel antagonist effects of spironolactone, an aldosterone antagonist. Am J Cardiol 1990;65(23):7K–8K discussion 3K.

[20] Haller H. Effective management of hypertension with dihydropyridine calcium channel blocker-based combination therapy in patients at high cardiovascular risk. Int J Clin Pract 2008;62(5):781–90.

[21] Yang B, Wu CN, Ji B, et al. Virtual population pharmacokinetic using physiologically based pharmacokinetic model for evaluating bioequivalence of oral lacidipine formulations in dogs. Asian J Pharm Sci 2017;12(1):98–104.

[22] Lehto P, Kortejarvi H, Liimatainen A, et al. Use of conventional surfactant media as surrogates for FaSSIF in simulating *in vivo* dissolution of BCS class II drugs. Eur J Pharm Biopharm 2011;78(3):531–8.

[23] Sun M, Wu C, Fu Q, et al. Solvent-shift strategy to identify suitable polymers to inhibit humidity-induced solid-state crystallization of lacidipine amorphous solid dispersions. Int J Pharm 2016;503(1–2):238–46.

[24] Sun MC, Li BY, Li YC, et al. Experimental observations and dissipative particle dynamic simulations on microstructures of pH-sensitive polymer containing amorphous solid dispersions. Int J Pharm 2017;517(1–2):185–95.

[25] Pan YH, Pang WZ, Lv J, Wang J, Yang CQ, Guo W. Solid state characterization of azelnidipine-oxalic acid co-crystal and co-amorphous complexes: The effect of different azelnidipine polymorphs. J Pharm Biomed Anal 2017;138:302–15.

[26] Walker G, Romann P, Poller B, et al. Probing pharmaceutical mixtures during milling: the potency of low-frequency Rraman spectroscopy in identifying disorder. Mol Pharm 2017;14(12):4675–84.

[27] Vigh T, Drávavölgyi G, Sóti PL, Pataki H, et al. Predicting final product properties of melt extruded solid dispersions from process parameters using Raman spectrometry. J Pharm Biomed Anal 2014;98:166–77.